Journal of Ionic Liquids 2 (2022) 100040

Contents lists available at ScienceDirect

Journal of Ionic Liquids

journal homepage: www.elsevier.com/locate/jil

Molecular dynamics study of the ionic liquid 1-*n*-hexyl-3-methylimidazolium *tris*(pentafluoroethyl)trifluorophosphate ([C_6C_1im][FAP]): Force field development and the effect of [FAP]$^-$ isomer content on properties

Ning Wang, Yong Zhang, Edward J. Maginn*

Department of Chemical and Biomolecular Engineering, University of Notre Dame, Notre Dame, IN 46556, USA

a r t i c l e i n f o

Keywords:
Molecular dynamics simulation
Ionic liquids
[FAP]$^-$ isomer

a b s t r a c t

A new all-atom force field for the *tris*(pentafluoroethyl)trifluorophosphate ([FAP]$^-$) anion was developed and paired with an existing force field for 1-*n*-hexyl-3-methylimidazolium ([C_6C_1im]$^+$). Molecular dynamics simulations were employed to compute the density, shear viscosity, self-diffusivity, local dynamics, and liquid structure of [C_6C_1im][FAP]. Computed densities, isothermal compressibility, isobaric expansivity, and shear viscosities all agree well with experimental data. The octahedral geometry of the [FAP]$^-$ anion results in facial ([fFAP]$^-$) and meridional ([mFAP]$^-$) isomers. Simulations with varying ratios of the two [FAP]$^-$ isomers show modest but non-negligible differences in properties as a function of isomer composition.

1. Introduction

The *tris*(perfluoroalkyl)trifluorophosphate ([FAP]$^-$) anion was introduced in 2005 by Ignat'ev et al., who demonstrated that when it is paired with a number of different classes of cations, it yields ionic liquids (ILs) that are hydrolytically stable when compared to more traditional ILs containing hexafluorophosphate ([PF_6]$^-$) or tetrafluoroborate ([BF_4]$^-$) anions (Ignat'ev et al., 2005). Several experimental studies (Li et al., 2011; Liu et al., 2010; Minami et al., 2008; Součková et al., 2012; Yao et al., 2009; Zaitsau and Verevkin, 2019) have been conducted to explore the physicochemical properties of [FAP]-based ILs. Properties such as density, viscosity, ionic conductivity, heat capacity, vapor pressure, and surface tension have been measured. Compared to ILs with the [PF_6]$^-$ or [BF_4]$^-$ anion, [FAP]-based ILs tend to have lower viscosities, higher ionic conductivities and molar heat capacities, and larger gravimetric densities. [FAP]-based ILs are miscible in organic solvents (Li et al., 2011) and are much more hydrophobic than conventional ILs, such that ILs containing a [FAP]$^-$ anion can be prepared with water contents of less than 15 ppm. In addition to low viscosity, [FAP]-based ILs tend to have high thermal and electrochemical stability and low melting points. These properties make them ideal for a number of different applications, including separations (Althuluth et al., 2012; Zhang et al., 2008), tribology (Li et al., 2013; Viesca et al., 2016), electrochemistry (Drüschler et al., 2011; Seki et al., 2012), and chemical synthesis (Ignat'ev et al., 2005).

The octahedral geometry of the [FAP]$^-$ anion results in two isomers: facial ([fFAP]$^-$) and meridional ([mFAP]$^-$); see Fig. 1. During the synthesis of the [FAP]$^-$ anion, *tris*(perfluoroalkyl)trifluorophosphoric acid ([$(C_2F_5)_3PF_3$]$^-$H$^+$ or [HFAP]) is formed. ^{19}F NMR measurements of [HFAP] suggest that 85 mol% of the [FAP]$^-$ anions are in the meridional form, while 15 mol% are in the facial form (Ignat'ev et al., 2005). This implies that ILs containing [FAP]$^-$ anions are actually isomeric mixtures, although only the [mFAP]$^-$ isomer was detected in ^{19}F NMR measurements of [C_8C_1IM][FAP]. Mao and Damodaran (2015); Mezger et al. (2013) showed using density functional theory (DFT) that [mFAP]$^-$ is more stable than [fFAP]$^-$ by 7.1 kJ/mol; the relatively small energy difference suggests that both isomers exist in solution. The DFT calculations also pointed to the existence of hydrogen bonds between [FAP]$^-$ and the imidazolium cation. Voroshylova et al. (2016) utilized DFT and infrared spectroscopy to investigate the electronic and structural properties of 1-ethyl-3-methylimidazolium *tris*(perfluoroethyl)trifluorophosphate ([C_2C_1im][FAP]). They also found that the [mFAP]$^-$ isomer was more stable, and that the coordination environment about the [C_2C_1im]$^+$ cation was different for the two different [FAP]$^-$ isomers. They found that [FAP]$^-$ can exist in multiple conformations at room temperature. The [fFAP]$^-$ isomer tends to stabilize its inter-ionic interactions with the cation due to its cup-shaped geometry where the three most negatively charged fluorine atoms are on the same side and lie closer to the cation than in [mFAP]$^-$. This raises the intriguing possibility that the

* Corresponding author.
E-mail addresses: nwang2@nd.edu (N. Wang), yzhang19@nd.edu (Y. Zhang), ed@nd.edu (E.J. Maginn).

https://doi.org/10.1016/j.jil.2022.100040
Received 27 May 2022; Received in revised form 15 July 2022; Accepted 15 July 2022
2772-4220/© 2022 The Authors. Published by Elsevier B.V. This is an open access article under the CC BY license (http://creativecommons.org/licenses/by/4.0/)

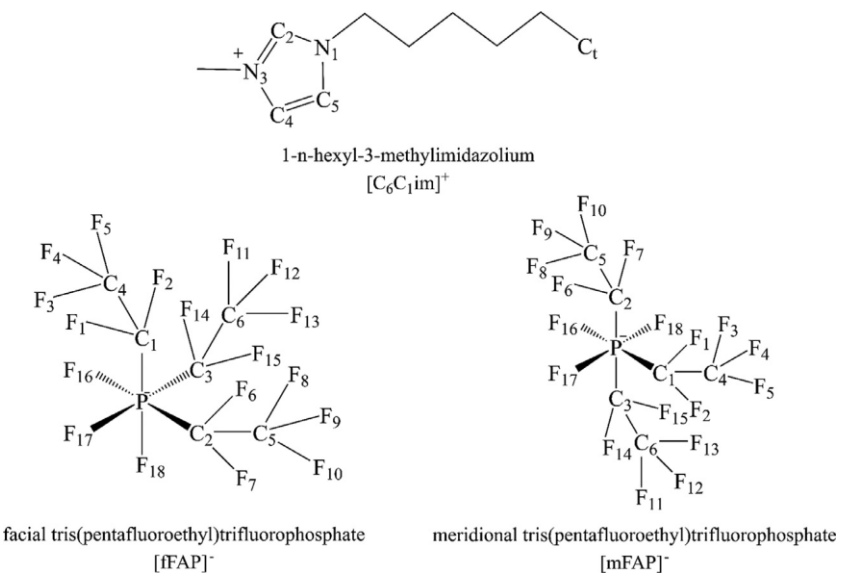

Fig. 1. 2D chemical structures and names of the cation $[C_6\ C_1\ im]^+$ (top), anion $[fFAP]^-$ (lower left), and anion $[mFAP]^-$ (lower right).

physical properties of ILs containing the $[FAP]^-$ anion could depend on the relative concentration of the two isomers. We are unaware of any physical property studies on [FAP]-based ILs that have examined this or even reported the isomeric composition.

Since the earliest days of contemporary IL research, molecular modeling and simulation have played an important role in helping understand and predict how thermophysical properties of ILs are related to their structure and chemical composition (Izgorodina et al., 2017; Jiang et al., 2019; Zhang et al., 2015b). Given the importance of [FAP]-based ILs, it is surprising that there are very few molecular simulation studies of ILs containing the $[FAP]^-$ anion, and no literature on how physical properties might depend on the two different $[FAP]^-$ isomers. Zhang et al. (2009) developed a united-atom force field for $[FAP]^-$ and computed CO_2 absorption isotherms in 1-*n*-hexyl-3-methylimidazolium ($[C_6C_1im]$) [FAP]. Their simulations helped explain why CO_2 is more soluble in $[C_6C_1im][FAP]$ than in $[C_6C_1im][PF_6]$. Shimizu et al. (2010) developed a new force field parameter set for generic fluoroalkylfluorophosphate ($[PF_y(C_mF_n)_x]^-$) anions based on the OPLS-AA force field. They used ab initio calculations to obtain missing bond, angle, and torsion parameters and partial charges. Then, they used molecular dynamics (MD) simulations to study the crystal structure of 1,3-dimethoxy-2-methylimidazolium $[FAP]^-$ and the liquid density of $[C_2C_1im][FAP]$ and $[C_4C_1iM][FAP]$. Their force field was able to capture experimental liquid densities to within 2–3%, but gave a crystal density that was almost 8% smaller than experiment. They attributed this to distortions in P-C-C angles caused by packing in the crystal phase, which were not accounted for in the force field. This force field was subsequently used to calculate the solubility of carbon dioxide, nitrous oxide, ethane, and nitrogen in $[C_2C_1im][FAP]$ and $[C_6C_1im][FAP]$, along with various site-site radial distribution functions for the IL (Almantariotis et al., 2012). Note that only the $[mFAP]^-$ isomer was considered in all of the simulations noted above. We are unaware of any simulation studies where a range of physical properties of [FAP]-based ILs were cpomputed and compared with experiment.

The objective of the present work is to develop and validate an all-atom force field for both the $[fFAP]^-$ and $[mFAP]^-$ isomers. The force field is based on the General Amber Force Field (GAFF) (Wang et al., 2004) to make it consistent with other IL force field parameterizations from our group, Lourenço et al. (2018); Zhang et al. (2015b) though it should be possible to adapt it for use with other popular IL force fields having a similar functional form Canongia Lopes et al. (2004); Doherty et al. (2017). We conduct MD simulations on $[C_6C_1im][FAP]$ at various temperatures and $[mFAP]^-$:$[fFAP]^-$ ratios to both test the accuracy of the $[FAP]^-$ force field and to determine the impact the anion isomer composition has on physical properties. Properties computed include density, isobaric expansivity, isothermal compressibility, self-diffusivity, shear viscosity, rotational dynamics, ion pair residence time, and liquid structure. Overall, the simulations agree with available experimental data reasonably well. We find that the anion isomer composition has a negligible effect on liquid structure, but it does have a small effect on liquid density and liquid dynamics. Computed shear viscosities match experimental data when a mixture of $[fFAP]^-$ and $[mFAP]^-$ anions are modeled.

2. Methods

2.1. Force field

Fig. 1 shows two-dimensional chemical structures and key atom labels of the $[C_6C_1im]^+$ cation and the two anion isomers $[fFAP]^-$ and $[mFAP]^-$.

The force field uses the GAFF functional form Wang et al. (2004)

$$E = \sum_{bonds} k_r(r-r_0)^2 + \sum_{angles} k_\theta(\theta-\theta_0)^2 + \sum_{torsions} k_\phi \times [1+\cos(n\phi-\gamma)] + \sum_{i=1}^{N-1}\sum_{j>i}^{N}\left\{4\varepsilon_{ij}\left[\left(\frac{\sigma_{ij}}{r_{ij}}\right)^{12}-\left(\frac{\sigma_{ij}}{r_{ij}}\right)^{6}\right]+\frac{q_iq_j}{4\pi\varepsilon_0 r_{ij}}\right\} \quad (1)$$

where E is the total potential energy of the system, k_r, k_θ, and k_ϕ are force constants; r_0, θ_0, and γ are nominal bond length, angle, and phase angle, respectively; n is periodicity; ε and σ are Lennard-Jones energy and size parameters; q_i and q_j are partial charges on atoms i and j; r_{ij} is the distance between atoms i and j at positions r_i and r_j; and ε_0 is the vacuum permittivity. The summation over torsion angles includes both conventional and improper dihedrals. Except where noted below, intramolecular bonded parameters as well as ε and σ were taken directly from GAFF. The structure of each isolated ion was optimized at the B3LYP/6-311++g(d,p) level using Gaussian 16 (Frisch et al., 2016). Partial charges for each atom were computed using the RESP method (Bayly et al., 1993). To account for polarizability and charge transfer in the condensed phase (Zhang and Maginn, 2012), the gas phase RESP partial charges were uniformly scaled by a factor of 0.8. For $[FAP]^-$, the nominal bond lengths and angles were determined from the optimized stuctures. The bond and angle force constants that are unavailable

in GAFF were adopted from a previous model for hexafluorophosphate ($[PF_6]^-$) (Liu et al., 2004). The parameters for the C-C-P-C dihedral in $[mFAP]^-$ and $[fFAP]^-$ were obtained by fitting to energy profiles computed at the B3LYP/6-311++g(d,p) level. Finally, the σ parameters in both $[mFAP]^-$ and $[fFAP]^-$ were scaled uniformly by a factor of 0.93 to better match the experimental density at 293 K (Almantariotis et al., 2012).A complete listing of force field parameters is provided in the Supplementary Material.

2.2. Simulation Procedure

MD simulations were conducted in the isothermal-isobaric (NPT) and canonical (NVT) ensembles using the LAMMPS package (Plimpton, 1995; Thompson et al., 2022). For each simulation, 400 $[C_6C_1im]^+$ cations were used together with 0, 100, 200, 300, or 400 $[fFAP]^-$ ions and 400, 300, 100, or 0 $[mFAP]^-$ ions, resulting in mixtures with $[fFAP]^-$ mole fractions of 0, 0.25, 0.5, 0.75, and 1. NPT simulations were performed at the following state points: 300 K, 1 atm; 300 K, 100 atm; 300 K, 200 atm; 300 K, 300 atm; 300 K, 500 atm; 350 K, 1 atm; 400 K, 1 atm; 450 K, 1 atm; and 500 K, 1 atm to obtain density. All NVT simulations were conducted at 300 K and 1 atm to obtain other properties. We used real units, periodic boundary conditions in all directions, and the Lorentz-Berthelot combining rule (Leach, 2001) for unlike atom interactions. The timestep was 1 fs. The cutoff of Lennard-Jones and Coulombic interactions was set to 12 Å. A standard Ewald summation method (Ewald, 1921) with an accuracy within 0.0001 and a particle-particle particle-mesh method (Hockney and Eastwood, 1988) with a desired relative error in forces within 0.0001 were used as the long-range electrostatics solver for NPT and NVT simulations, respectively. Temperature and pressure were maintained by the Nosé-Hoover (Hoover, 1985) thermostat and the extended Lagrangian (Shinoda et al., 2004) barostat, respectively. Initial configurations were generated by inserting ions into a cubic box using Packmol (Martínez and Martínez, 2003; Martínez et al., 2009). Energy minimization was then carried out to relax the initial high energy state. A maximum of 10,000 interations were used. The stopping tolerance for energy and force was 0.0001 and 0.000001, respectively. Following the minimization, NPT simulations were carried out for 2 ns to reach the desired average volume followed by an 8 ns production run, which was used to compute the density. Finally, thirty independent 10 ns NVT production runs were conducted at the average density for dynamic analysis and a single 30 ns NVT simulation was used for structural analysis.

3. Results and discussions

3.1. Density

Densities as a function of temperature and pressure were calculated from the NPT simulations and are plotted in Fig. 2. We divided the converged part of the NPT production runs into three blocks and took the block average as the reported density. Uncertainties were assumed to be equal to the standard deviation, computed as

$$\sigma = \sqrt{\frac{\sum_{i=1}^{n} (\bar{\rho}_i - \frac{\sum_{i=1}^{n} \bar{\rho}_i}{n})^2}{n}} \quad (2)$$

where n is the number of blocks, and $\bar{\rho}_i$ is the average density of block i. As expected, density decreases with increasing temperature and increases with increasing pressure; both follow a linear relation. There are several experimental reports of the density of $[C_6C_1im][FAP]$ (Akbar et al., 2016; Almantariotis et al., 2012; Jacquemin et al., 2008; Li et al., 2011; Součková et al., 2012). The agreement between measurements is excellent, with deviations within 0.045%. We therefore use one set of experimental data when comparing with simulations (Almantariotis et al., 2012). Compared with experiments, the MD simulations slightly underestimate the density, with a deviation of less than 3.5%. Computed density, standard deviation, and deviation from experiments for each state point are provided in Table S1 of the Supplementary Material. The simulations predict that the isomeric mixture of $[C_6C_1im][FAP]$ behaves like an ideal solution. That is, the density of the mixture is approximately equal to the weighted average densities of pure $[C_6C_1im][fFAP]$ and $[C_6C_1im][mFAP]$. The density of $[C_6C_1im][mFAP]$ is slightly higher than $[C_6C_1im][fFAP]$, and the density of the mixture slightly decreases with an increase in the fraction of the $[fFAP]^-$ anion.

Table 1
Isobaric expansivity and isothermal compressibility of $[C_6C_1im][FAP]$ with different mole fraction of isomers.

	$\alpha_P \times 10^{-4} (\frac{1}{K})$	$\kappa_T \times 10^{-4} (\frac{1}{MPa})$
Expt.	7.0	5.5
$x_{[fFAP]^-}$ =0	8.5	5.1
$x_{[fFAP]^-}$ =0.25	8.6	5.0
$x_{[fFAP]^-}$ =0.5	8.5	5.0
$x_{[fFAP]^-}$ =0.75	8.5	5.0
$x_{[fFAP]^-}$ =1	8.5	5.1
Mean Difference	21.7%	−8.4%

Qualitatively, the MD simulations capture the trends in density with temperature and pressure quite well. To make the comparison more quantitative, least squares linear fits were applied to the simulation results to calculate the isobaric expansivity (α_P) and isothermal compressibility (κ_T) from the thermodynamic expressions

$$\alpha_P = V^{-1}(\partial V/\partial T)_P = -\rho^{-1}(\partial \rho/\partial T)_P = -(\partial \ln \rho/\partial T)_P \quad (3)$$

$$\kappa_T = -V^{-1}(\partial V/\partial P)_T = \rho^{-1}(\partial \rho/\partial P)_T = (\partial \ln \rho/\partial P)_T \quad (4)$$

Table 1 shows a comparison of the simulated and experimental expansivity and compressibility. The average deviation or mean difference from experiment is 10–20%, which is reasonable considering that these are derivative quantities that are small in magnitude. The values of α_P and κ_T show little dependence on the anion isomer composition.

3.2. Shear viscosity

The shear viscosity was calculated from NVT simulations using a time decomposition method (Zhang et al., 2015a), in which thirty independent trajectories were run at the same condition but with different initial velocities. The viscosity of each trajectory was computed from Allen and Tildesley (2017)

$$\eta = \frac{V}{6k_B T} \sum_{\alpha \leq \beta} \int_0^\infty \langle P_{\alpha\beta}(t) \cdot P_{\alpha\beta}(0) \rangle dt \quad (5)$$

where V is the box volume, T is the temperature, k_B is the Boltzmann constant, and $P_{\alpha\beta}$ is the modified pressure tensor: $P_{xy} = P_{xy}$, $P_{yz} = P_{yz}$, $P_{xz} = P_{xz}$, $P_{xx} = 0.5(P_{xx} - P_{yy})$, $P_{yy} = 0.5(P_{yy} - P_{zz})$, and $P_{zz} = 0.5(P_{xx} - P_{zz})$. The final viscosity value was obtained by performing a weighted fit of the average over thirty simulations as a function of time to a double exponential function. The uncertainty in the calculated viscosity was estimated from a bootstrapping method by randomly re-sampling these thirty trajectories with replacement (Zhang et al., 2018). Notably, the final viscosity depends on the number of bootstrapping trials. As shown in Figure S1, the value of viscosity starts to converge when the number of bootstrapping trials is greater than 20. To better estimate the final value and the corresponding uncertainty, we decide to use results from 30 trials to represent the final reported value. Detailed values are provided in Table S2 of the Supplementary Material. Surprisingly, Fig. 3 shows that the computed viscosity of the IL having 50% $[fFAP]^-$ isomers are higher than those of both pure $[C_6C_1im][mFAP]$ and pure $[C_6C_1im][fFAP]$ and are very close to the experimental values. Values for viscosity at $x_{[fFAP]^-}$ = 0, 0.25, 0.75, and 1 are insensitive to isomer mole fraction. The simulations therefore suggest that the viscosity of ILs with 50% $[fFAP]^-$ isomer is slightly higher than the ILs with either pure $[mFAP]^-$ or $[fFAP]^-$ anions. We caution, however, that the error bars in

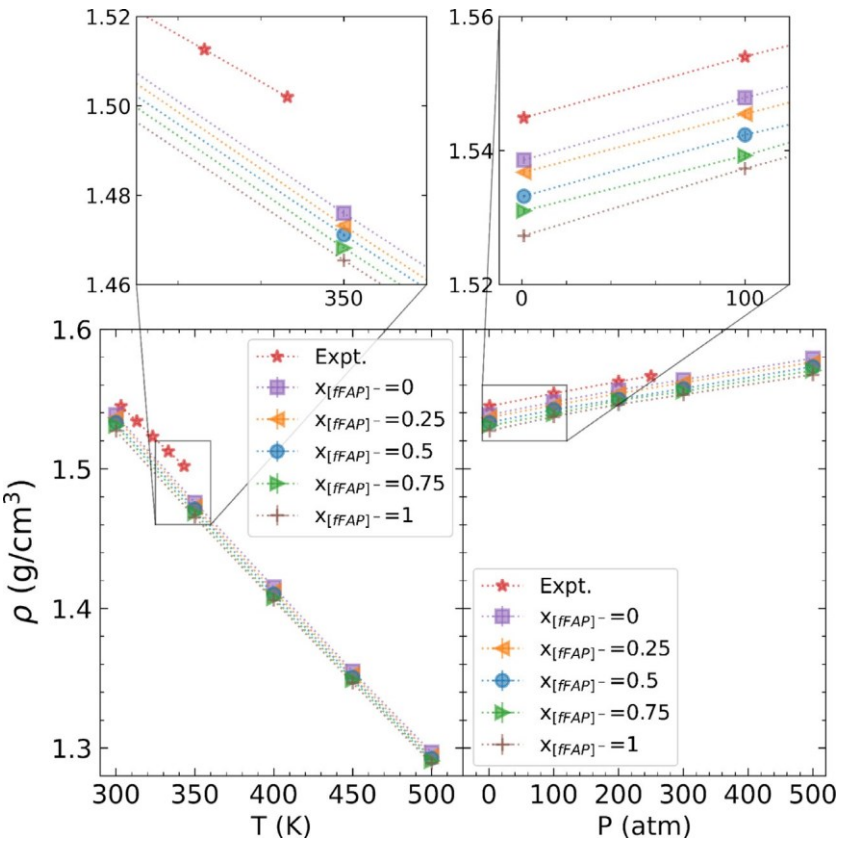

Fig. 2. Density of [C_6 C_1 im][FAP] with different mole fraction of [fFAP]⁻ and [mFAP]⁻ vs. temperature at 1 atm (left) and vs. pressure (right) at 300 K (simulation) and 303.18 K (experiment) (Almantariotis et al., 2012).

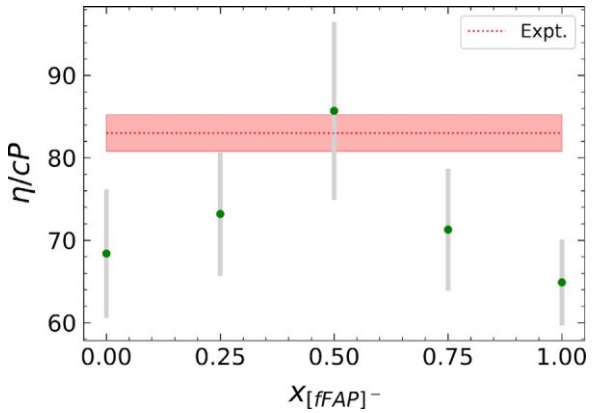

Fig. 3. Computed shear viscosity of [C_6 C_1 im][FAP] as a function of [fFAP]⁻ isomer mole fraction at 300 K compared with an average of multiple experimental results (Almantariotis et al., 2012; Dutt, 2010; Li et al., 2011) interpolated to 300 K using the Vogel–Fulcher–Tammann equation. The red dotted line represents the average of experimental values, and the width of the red shaded region refers to one standard deviation between different experiments. (For interpretation of the references to color in this figure legend, the reader is referred to the web version of this article.)

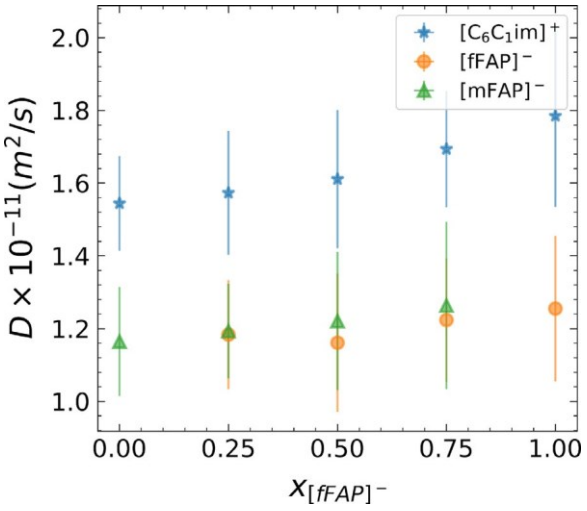

Fig. 4. Computed self-diffusivity of [C_6 C_1 im][FAP] versus mole fraction of [fFAP]⁻ at 300 K.

computed viscosity are large and so any trend with isomer composition is difficult to establish with certainty. It would be interesting, however, to see if this prediction holds up to experimental scrutiny, which would require additional experiments on the pure isomers.

3.3. Self-diffusivity

As an assessment of translational dynamics, the self-diffusivity was computed by fitting the linear region of the mean squared displacement (MSD) versus time according to the Einstein equation (Allen and Tildesley, 2017) using the PyLAT package (Humbert et al., 2019). Values were computed as the average over thirty independent simulations, and error bars for ILs with different $x_{[fFAP]^-}$ were estimated as the standard deviation of the thirty simulations. The final reported values accounting for the system-size correction using the approach of Yeh and Hummer (2004) are documented in Table S3. As shown in Fig. 4, the simulations predict that the $[C_6C_1im]^+$ cation diffuses faster than both anions. In the mixture, [mFAP]⁻ and [fFAP]⁻ have similar self-diffusivities, within the uncertainty of the calculations. There is a slight increase in self-diffusivity as the concentration of [fFAP]⁻ increases, but the trend

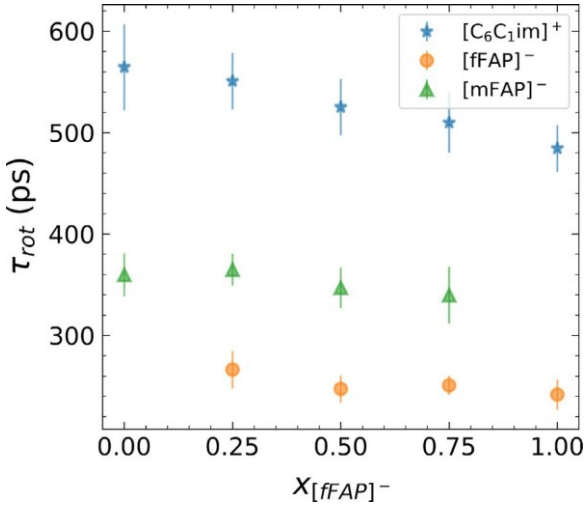

Fig. 5. Rotational time constant calculated from rotational correlation function using N_1-N_3 as the vector for [C_6 C_1 im] (blue) and C_2-C_3 as the vector for $[fFAP]^-$ (orange) and $[mFAP]^-$ (green) as a function of $[fFAP]^-$ isomer mole fraction at 300 K. (For interpretation of the references to color in this figure legend, the reader is referred to the web version of this article.)

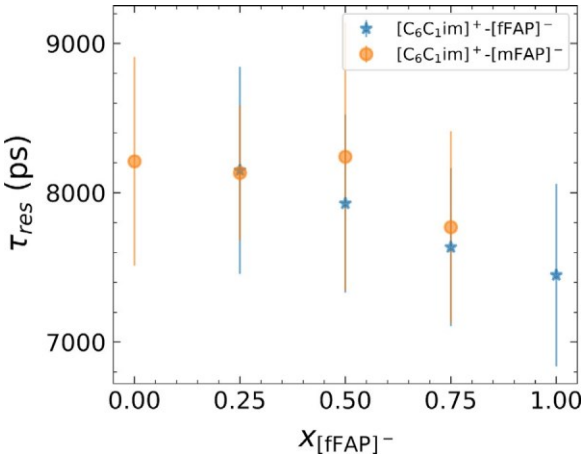

Fig. 6. Residence time of [C_6 C_1 im]$^+$-$[FAP]^-$ interaction as a function of $[fFAP]^-$ isomer mole fraction at 300 K.

is modest. More interesting is the fact that the self-diffusivity trend does not follow the inverse of the viscosity trend. That is, the viscosity results would suggest that the pure $[mFAP]^-$ and $[fFAP]^-$ systems have higher self-diffusivities than the mixtures, but this is not the case. Thus simple Stokes–Einstein behavior is not observed in these mixtures. Unfortunately, we are unaware of any experimental self-diffusivity data against which to compare the simulation results.

3.4. Rotational dynamics

To study the rotational dynamics of $[C_6C_1im][FAP]$ with different mole fractions of the facial and meridional isomers, the rotational correlation function $C(t)$ was computed for the cation and anion as

$$C(t) = \langle \frac{1}{2}[3cos^2\theta_i(t) - 1] \rangle \quad (6)$$

where $\theta_i(t)$ is the angle between a vector in a given ion i at time 0 and at time t (Wu et al., 2011). The time constant τ_{rot} was determined by fitting the correlation function to a multi-exponential function

$$C(t) = \sum_i A_i \times exp(-t/B_i) \quad (7)$$

with 1 to 4 terms used for different systems and integrating the fitting result from time 0 to infinity.

$$\tau_{rot} = \int_0^\infty C(t)dt \quad (8)$$

The vector chosen for $[C_6C_1im]^+$ is the one connecting N_1 and N_3 in the plane of the ring, and the vectors chosen for $[fFAP]^-$ and $[mFAP]^-$ connect atoms C_2 and C_3, as shown in Fig. 1. Computed time constants were obtained from thirty independent simulations for each data point, and the corresponding uncertainty was estimated from the standard deviation of these thirty independent simulations. Detailed values are listed in Table S4. As shown in Fig. 5, the relative order of rotational time constant for different ions follows: $[C_6C_1im]^+$ > $[mFAP]^-$ > $[fFAP]^-$. The larger the time constant, the slower the ion rotates. Thus, $[fFAP]^-$ rotates slightly faster than $[mFAP]^-$ because of $[mFAP]^-$'s relatively longer rotational axis, and the cation rotates much more slowly than either anion. We believe this is due to relatively long alkyl chain on the cation hindering rotation of the cation ring. Time constants for all three ions decrease modestly with increasing $[fFAP]^-$ mole fraction, meaning that the addition of $[fFAP]^-$ will slightly enhance the rotational dynamics of the IL; this is consistent with the slight increase in self-diffusivity observed with increasing $[fFAP]^-$ concentration. Overall, considering the uncertainty, the decreasing trend is modest, and the rotational dynamics has a weak dependence on anion composition.

3.5. Residence time

The average residence time of all anions in the first solvation shell of a cation (or vice versa) was determined by computing the residence time autocorrelation function (RTACF) $R(t)$

$$R(t) = \frac{\langle H(0)H(t) \rangle}{\langle H \rangle} \quad (9)$$

where $H(t)$ equal to 1 means an anion (cation) is still in the first solvation shell about a central cation (anion) after elapsed time t, while $H(t)$ equal to 0 means the counterion has been exchanged from the first solvation shell over time t. The residence time correlation function was fit to a multi-exponential function like that in Eq. (7) and the residence time was evaluated from the infinite time integral as in Eq. (8). Residence times were computed from the average of thirty independent simulations, and the corresponding error bars were estimated from the standard deviation of the thirty independent simulations. Numerical values are provided in Table S5. As shown in Fig. 6, the residence times of both $[C_6C_1im]^+$-$[mFAP]^-$ and $[C_6C_1im]^+$-$[fFAP]^-$ decrease slightly with increasing concentration of $[fFAP]^-$ in the mixture. The differences in residence times between the two anions are small. These results are consistent with the self-diffusivity and rotational dynamics trends, in which dynamics increase slightly as $[fFAP]^-$ composition increases.

3.6. Effect of isomer composition on liquid structure

3.6.1. Radial distribution functions

The center of mass (COM) radial distribution function (RDF) was calculated using the PyLAT package (Humbert et al., 2019) to study the effect of isomer composition on liquid structure. Fig. 7 shows the typical charge alternation structure common to ILs. Very little difference is observed as a function of anion isomer composition, which is consistent with the ideal mixing observed with density.

Since COM RDF sometimes cannot provide detailed insight on specific molecular interactions, various site-to-site partial RDFs were also computed. In Fig. 8, we focus on the C_2 carbon on the ring of the cation, the F_3 fluorine at the end of the alkyl chain of the anion, and the F_{16} fluorine directly connected to the central phosphorus (P) of the anion. The intensity of the first peak for C_2-F_{16} interactions is greater than that for C_2-F_3, suggesting that the positive cation prefers to sit close to the negatively charged central P atom of the anion. Once again, there is very

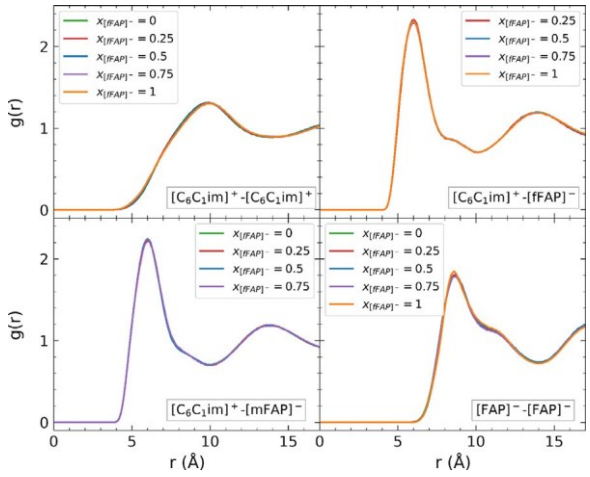

Fig. 7. Computed center of mass RDF of [C_6 C_1 im][FAP] with different mole fraction of [FAP]$^-$ isomer at 300 K. [FAP]$^-$-[FAP]$^-$ interaction refers to [mFAP]$^-$-[mFAP]$^-$ for $x_{[fFAP]^-}$=0, [fFAP]$^-$-[mFAP]$^-$ for $x_{[fFAP]^-}$ = 0.25, 0.5, and 0.75, and [fFAP]$^-$-[fFAP]$^-$ for $x_{[fFAP]^-}$ = 1.

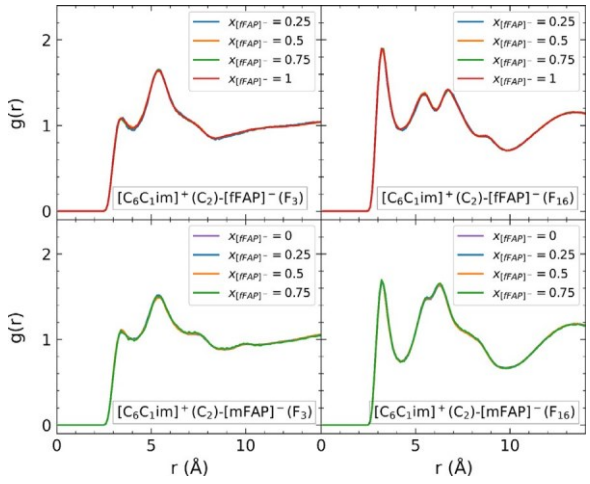

Fig. 8. Computed partial RDF of [C_6 C_1 im][FAP] with different mole fraction of [FAP]$^-$ isomer at 300 K.

little difference between the partial RDFs for the two anions, consistent with ideal mixing behavior.

3.6.2. Structure factor

Finally, both the X-ray and the neutron total structure factors were computed using the following expression

$$S(q) = \frac{\rho_0 \sum_{i=1}^{n}\sum_{j=1} x_i x_j f_i(q) f_j(q) \int_0^\infty 4\pi r^2 (g_{ij}(r) - 1) \frac{\sin(qr)}{qr} w(r) dr}{[\sum_{i=1} x_i f_i(q)]^2} \quad (10)$$

where ρ_0 is the number density, x_i and x_j are the fractions of atom types i and j, respectively, n is the total number of atom types, $f(q)$ is the X-ray form factor or neutron scattering length (which is independent of q), r is the distance between two atoms, $g_{ij}(r)$ is the RDF between sites i and j, q is the scattering factor, and $w(r)$ is the Lorch window function to mitigate finite truncation effects (Kashyap et al., 2012; Kaur et al., 2016). To examine the decomposed cation-cation, cation-anion, and anion-anion correlations, the total structure factor was partitioned conforming to the following rule. For pure [C_6C_1im][fFAP] or [C_6C_1im][mFAP],

$$S^{total}(q) = S^{[C_6C_1im]^+-[C_6C_1im]^+}(q) + S^{[C_6C_1im]^+-[FAP]^-}(q) + S^{[FAP]^--[FAP]^-}(q) \quad (11)$$

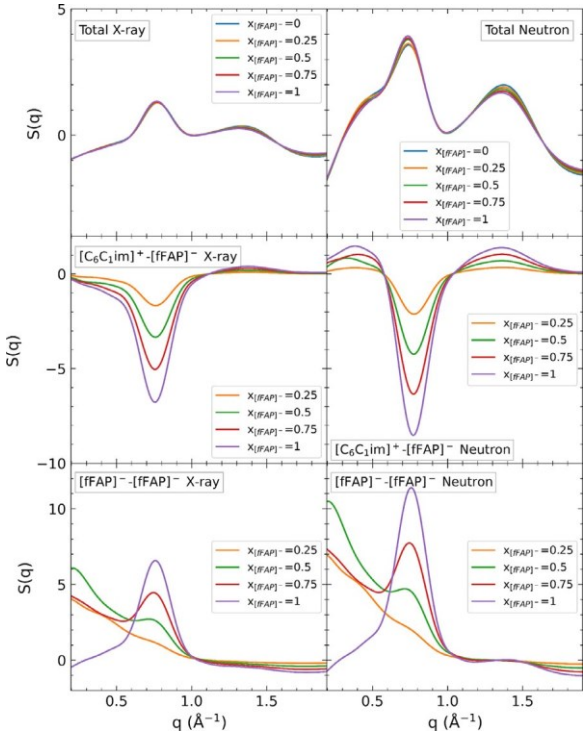

Fig. 9. The computed total and decomposed X-ray (left) and neutron (right) structure factors of [C_6 C_1 im][FAP] with different mole fraction of [FAP]$^-$ isomer at 300 K.

For [C_6C_1im][FAP] mixtures with different isomer composition,

$$S^{total}(q) = S^{[C_6C_1im]^+-[C_6C_1im]^+}(q) + S^{[C_6C_1im]^+-[fFAP]^-}(q) + S^{[C_6C_1im]^+-[mFAP]^-}(q) + S^{[fFAP]^--[fFAP]^-}(q) + S^{[fFAP]^--[mFAP]^-}(q) + S^{[mFAP]^--[mFAP]^-}(q) \quad (12)$$

The calculated total and decomposed X-ray and neutron structure factors of [C_6C_1im][FAP] are shown in Fig. 9 and Figure S2. Total X-ray and neutron structure factors include a charge alternation peak and an adjacency peak (Araque et al., 2015). The highest peak in the total structure factor is the peak at 0.74 Å^{-1} which is associated with charge alternation. [C_6C_1im]$^+$-[fFAP]$^-$, [C_6C_1im]$^+$-[mFAP]$^-$, [fFAP]$^-$-[fFAP]$^-$, and [mFAP]$^-$-[mFAP]$^-$ subcomponents make a crucial contribution to the total S(q). The charge alternation peak is positive for ions with the same charge and is negative for ions with opposite charge. With increasing mole fraction of the [fFAP]$^-$ isomer, the intensity for [C_6C_1im]$^+$-[fFAP]$^-$ and [fFAP]$^-$-[fFAP]$^-$ increases whereas the intensity for [C_6C_1im]$^+$-[mFAP]$^-$ and [mFAP]$^-$-[mFAP]$^-$ decreases due to the concentration effect. The peak at 1.37 Å^{-1} is an indication of adjacency correlation of neighboring atoms. It is interesting to notice that, for [C_6C_1im][FAP] with different isomers, both [fFAP]$^-$-[fFAP]$^-$ and [mFAP]$^-$-[mFAP]$^-$ contributions show a positive signal at around 0.2 Å^{-1}. The length scale of this signal is similar to the polar-nonpolar alternation structure reported previously for other ILs (Annapureddy et al., 2010; Araque et al., 2015). However, detailed study of this structure needs a much larger simulation box, which will be explored in future studies. Overall, the total S(q) presented in the current study shows no composition dependence, but most subcomponents do change with isomer composition.

4. Conclusion

A new GAFF-based force field parameter set was developed for both the facial and the meridional isomers of the *tris*(pentafluoroethyl)trifluorophosphate anion ([fFAP]$^-$ and [mFAP]$^-$,

respectively). The new FAP force field was able to capture experimental density and viscosity of the IL $[C_6C_1im][FAP]$ reasonably well, when paired with a previously validated force field for $[C_6C_1im]^+$.

Because ILs containing the $[FAP]^-$ anion are typically composed of a mixture of the two anion isomers, the effect of $[FAP]^-$ isomer composition on the physical and structural properties of $[C_6C_1im][FAP]$ was studied. The liquid structure showed essentially no difference as a function of anion isomer composition, suggesting an ideal mixture. Interestingly, however, liquid density and dynamical properties did show a slight dependence on isomer composition. Liquid density shows a subtle decrease with increasing $[fFAP]^-$ isomer composition. Self-diffusivity, ion rotational dynamics, and ion pair exchange dynamics all became slightly faster as the fraction of the $[fFAP]^-$ isomer increased. The computed viscosity of $[C_6C_1im][FAP]$ having $[fFAP]^-$ mole fractions of 0.5 agreed remarkably well with experimental data. Interestingly, the viscosities of pure $[C_6C_1im][fFAP]$ and $[C_6C_1im][mFAP]$ were lower than those of the isomer mixtures, suggesting that the dynamics of the mixture do not follow a simple Stokes–Einstein model. We hope these findings stimulate additional experimental investigations of ILs containing this important anion.

Declaration of Competing Interest

The authors declare that they have no known competing financial interests or personal relationships that could have appeared to influence the work reported in this paper.

Acknowledgments

We greatly appreciate the financial support provided by the National Science Foundation, EFRI DChem: Next-generation Low Global Warming Refrigerants, Award no. EFRI-2029354 and the computing resources from the Center for Research Computing (CRC) at the University of Notre Dame.

Supplementary material

Supplementary material associated with this article can be found, in the online version, at 10.1016/j.jil.2022.100040

References

Akbar, M.M., Chemat, F., Arunagiri, A., Murugesan, T., 2016. Density and excess properties of *N*-methyldiethanolamine (MDEA) with 1-hexyl-3-methylimidazolium tris (pentafluoroethyl) trifluorophosphate [hmim][FAP]. J. Therm. Anal. Calorim. 123 (1), 785–791. doi:10.1007/s10973-015-4957-6.

Allen, M., Tildesley, D., 2017. Computer Simulation of Liquids. Oxford University Press. https://books.google.com/books?id=WFExDwAAQBAJ

Almantariotis, D., Stevanovic, S., Fandiño, O., Pensado, A.S., Padua, A.A.H., Coxam, J.-Y., Costa Gomes, M.F., 2012. Absorption of carbon dioxide, nitrous oxide, ethane and nitrogen by 1-alkyl-3-methylimidazolium (C_n mim, n = 2, 4, 6) tris(pentafluoroethyl)trifluorophosphate ionic liquids (eFAP). J. Phys. Chem. B 116 (26), 7728–7738. doi:10.1021/jp304501p.

Althuluth, M., Mota-Martinez, M.T., Kroon, M.C., Peters, C.J., 2012. Solubility of carbon dioxide in the ionic liquid 1-ethyl-3-methylimidazolium tris(pentafluoroethyl)trifluorophosphate. J. Chem. Eng. Data 57 (12), 3422–3425. doi:10.1021/je300521y.

Annapureddy, H.V.R., Kashyap, H.K., De Biase, P.M., Margulis, C.J., 2010. What is the origin of the prepeak in the X-ray scattering of imidazolium-based room-temperature ionic liquids? J. Phys. Chem. B 114, 16838–16846. doi:10.1021/jp108545z.

Araque, J.C., Hettige, J.J., Margulis, C.J., 2015. Modern room temperature ionic liquids, a simple guide to understanding their structure and how it may relate to dynamics. J. Phys. Chem. B 119 (40), 12727–12740. doi:10.1021/acs.jpcb.5b05506.

Bayly, C.I., Cieplak, P., Cornell, W., Kollman, P.A., 1993. A well-behaved electrostatic potential based method using charge restraints for deriving atomic charges: the RESP model. J. Phys. Chem. 97 (40), 10269–10280. doi:10.1021/j100142a004.

Canongia Lopes, J.N., Deschamps, J., Pádua, A.A.H., 2004. Modeling ionic liquids using a systematic all-atom force field. J. Phys. Chem. B 108 (6), 2038–2047. doi:10.1021/jp0362133.

Doherty, B., Zhong, X., Gathiaka, S., Li, B., Acevedo, O., 2017. Revisiting OPLS force field parameters for ionic liquid simulations. J. Chem. Theory Comput. 13 (12), 6131–6145. doi:10.1021/acs.jctc.7b00520.

Drüschler, M., Huber, B., Roling, B., 2011. On capacitive processes at the interface between 1-ethyl-3-methylimidazolium tris(pentafluoroethyl)trifluorophosphate and Au(111). J. Phys. Chem. C 115 (14), 6802–6808. doi:10.1021/jp200395j.

Dutt, G.B., 2010. Influence of specific interactions on the rotational dynamics of charged and neutral solutes in ionic liquids containing tris(pentafluoroethyl)trifluorophosphate (FAP) anion. J. Phys. Chem. B 114 (27), 8971–8977. doi:10.1021/jp1039282.

Ewald, P.P., 1921. Die berechnung optischer und elektrostatischer gitterpotentiale. Ann. Phys. (Berlin, Ger.) 369 (3), 253–287. doi:10.1002/andp.19213690304.

Frisch, M. J., Trucks, G. W., Schlegel, H. B., Scuseria, G. E., Robb, M. A., Cheeseman, J. R., Scalmani, G., Barone, V., Petersson, G. A., Nakatsuji, H., Li, X., Caricato, M., Marenich, A. V., Bloino, J., Janesko, B. G., Gomperts, R., Mennucci, B., Hratchian, H. P., Ortiz, J. V., Izmaylov, A. F., Sonnenberg, J. L., Williams-Young, D., Ding, F., Lipparini, F., Egidi, F., Goings, J., Peng, B., Petrone, A., Henderson, T., Ranasinghe, D., Zakrzewski, V. G., Gao, J., Rega, N., Zheng, G., Liang, W., Hada, M., Ehara, M., Toyota, K., Fukuda, R., Hasegawa, J., Ishida, M., Nakajima, T., Honda, Y., Kitao, O., Nakai, H., Vreven, T., Throssell, K., Montgomery Jr., J. A., Peralta, J. E., Ogliaro, F., Bearpark, M. J., Heyd, J. J., Brothers, E. N., Kudin, K. N., Staroverov, V. N., Keith, T. A., Kobayashi, R., Normand, J., Raghavachari, K., Rendell, A. P., Burant, J. C., Iyengar, S. S., Tomasi, J., Cossi, M., Millam, J. M., Klene, M., Adamo, C., Cammi, R., Ochterski, J. W., Martin, R. L., Morokuma, K., Farkas, O., Foresman, J. B., Fox, D. J., 2016. Gaussian 16, Revision C.01. Gaussian Inc. Wallingford CT. https://gaussian.com/gaussian16/.

Hockney, R., Eastwood, J., 1988. Computer Simulation Using Particles. Taylor & Francis. https://books.google.com/books?id=8JQvngEACAAJ

Hoover, W.G., 1985. Canonical dynamics: equilibrium phase-space distributions. Phys. Rev. A 31 (3), 1695. doi:10.1103/PhysRevA.31.1695.

Humbert, M.T., Zhang, Y., Maginn, E.J., 2019. PyLAT: Python LAMMPS analysis tools. J. Chem. Inf. Model. 59 (4), 1301–1305. doi:10.1021/acs.jcim.9b00066.

Ignat'ev, N., Welz-Biermann, U., Kucheryna, A., Bissky, G., Willner, H., 2005. New ionic liquids with tris(perfluoroalkyl)trifluorophosphate (FAP) anions. J. Fluorine Chem. 126 (8), 1150–1159. doi:10.1016/j.jfluchem.2005.04.017.

Izgorodina, E.I., Seeger, Z.L., Scarborough, D.L.A., Tan, S.Y.S., 2017. Quantum chemical methods for the prediction of energetic, physical, and spectroscopic properties of ionic liquids. Chem. Rev. 117 (10), 6696–6754. doi:10.1021/acs.chemrev.6b00528.

Jacquemin, J., Ge, R., Nancarrow, P., Rooney, D.W., Costa Gomes, M.F., Pádua, A.A.H., Hardacre, C., 2008. Prediction of ionic liquid properties. I. Volumetric properties as a function of temperature at 0.1 MPa. J. Chem. Eng. Data 53 (3), 716–726. doi:10.1021/je700707y.

Jiang, K., Liu, L., Liu, X., Zhang, X., Zhang, S., 2019. Insight into the relationship between viscosity and hydrogen bond of a series of imidazolium ionic liquids: A molecular dynamics and density functional theory study. Ind. Eng. Chem. Res. 58 (40), 18848–18854. doi:10.1021/acs.iecr.9b02535.

Kashyap, H.K., Santos, C.S., Annapureddy, H.V., Murthy, N.S., Margulis, C.J., Castner Jr., E.W., 2012. Temperature-dependent structure of ionic liquids: X-ray scattering and simulations. Faraday Discuss. 154, 133–143. doi:10.1039/C1FD00059D.

Kaur, S., Gupta, A., Kashyap, H.K., 2016. Nanoscale spatial heterogeneity in deep eutectic solvents. J. Phys. Chem. B 120 (27), 6712–6720. doi:10.1021/acs.jpcb.6b04187.

Leach, A., 2001. Molecular Modelling: Principles and Applications. Prentice Hall. https://books.google.com/books?id=kB7jsbV-uhkC

Li, H., Rutland, M.W., Atkin, R., 2013. Ionic liquid lubrication: influence of ion structure, surface potential and sliding velocity. Phys. Chem. Chem. Phys. 15, 14616–14623. doi:10.1039/C3CP52638K.

Li, J.-G., Hu, Y.-F., Ling, S., Zhang, J.-Z., 2011. Physicochemical properties of $[C_6\,mim][PF_6]$ and $[C_6\,mim][(C_2F_5)_3PF_3]$ ionic liquids. J. Chem. Eng. Data 56 (7), 3068–3072. doi:10.1021/je200073x.

Liu, Q.-S., Tong, J., Tan, Z.-C., Welz-Biermann, U., Yang, J.-Z., 2010. Density and surface tension of ionic liquid $[C_2mim][PF_3(CF_2CF_3)_3]$ and prediction of properties $[C_nmim][PF_3(CF_2CF_3)_3]$ (n = 1, 3, 4, 5, 6). J. Chem. Eng. Data 55 (7), 2586–2589. doi:10.1021/je901035d.

Liu, Z., Huang, S., Wang, W., 2004. A refined force field for molecular simulation of imidazolium-based ionic liquids. J. Phys. Chem. B 108, 12978–12989. doi:10.1021/jp048369o.

Lourenço, T.C., Zhang, Y., Costa, L.T., Maginn, E.J., 2018. A molecular dynamics study of lithium-containing aprotic heterocyclic ionic liquid electrolytes. J. Chem. Phys. 148 (19), 193834. doi:10.1063/1.5016276.

Mao, J.X., Damodaran, K., 2015. Spectroscopic and computational analysis of the molecular interactions in the ionic liquid $[Emim]^+[FAP]^-$. Ionics 21 (6), 1605–1613. doi:10.1007/s11581-014-1341-7.

Martínez, J.M., Martínez, L., 2003. Packing optimization for automated generation of complex system's initial configurations for molecular dynamics and docking. J. Comput. Chem. 24 (7), 819–825. doi:10.1002/jcc.10216.

Martínez, L., Andrade, R., Birgin, E.G., Martínez, J.M., 2009. PACKMOL: a package for building initial configurations for molecular dynamics simulations. J. Comput. Chem. 30 (13), 2157–2164. doi:10.1002/jcc.21224.

Mezger, M., Ocko, B.M., Reichert, H., Deutsch, M., 2013. Surface layering and melting in an ionic liquid studied by resonant soft X-ray reflectivity. Proc. Natl. Acad. Sci. USA 110 (10), 3733–3737. doi:10.1073/pnas.1211749110.

Minami, I., Kita, M., Kubo, T., Nanao, H., Mori, S., 2008. The tribological properties of ionic liquids composed of trifluorotris (pentafluoroethyl) phosphate as a hydrophobic anion. Tribol. Lett. 30 (3), 215–223. doi:10.1007/s11249-008-9329-y.

Plimpton, S., 1995. Fast parallel algorithms for short-range molecular dynamics. J. Comput. Phys. 117 (1), 1–19. doi:10.1006/jcph.1995.1039.

Seki, S., Serizawa, N., Hayamizu, K., Tsuzuki, S., Umebayashi, Y., Takei, K., Miyashiro, H., 2012. Physicochemical and electrochemical properties of 1-ethyl-3-methylimidazolium tris(pentafluoroethyl)trifluorophosphate and 1-ethyl-3-

methylimidazolium tetracyanoborate. J. Electrochem. Soc. 159 (7), A967–A971. doi:10.1149/2.032207jes.

Shimizu, K., Almantariotis, D., Gomes, M.F.C., Pádua, A.A.H., Canongia Lopes, J.N., 2010. Molecular force field for ionic liquids V: hydroxyethylimidazolium, dimethoxy-2- methylimidazolium, and fluoroalkylimidazolium cations and bis(fluorosulfonyl)amide, perfluoroalkanesulfonylamide, and fluoroalkylfluorophosphate anions. J. Phys. Chem. B 114 (10), 3592–3600. doi:10.1021/jp9120468.

Shinoda, W., Shiga, M., Mikami, M., 2004. Rapid estimation of elastic constants by molecular dynamics simulation under constant stress. Phys. Rev. B 69, 134103. doi:10.1103/PhysRevB.69.134103.

Součková, M., Klomfar, J., Pátek, J., 2012. Temperature dependence of the surface tension and 0.1 MPa density for 1-C_n -3-methylimidazolium tris(pentafluoroethyl)trifluorophosphate with n = 2, 4, and 6. J. Chem. Thermodyn. 48, 267–275. doi:10.1016/j.jct.2011.12.033.

Thompson, A.P., Aktulga, H.M., Berger, R., Bolintineanu, D.S., Brown, W.M., Crozier, P.S., in 't Veld, P.J., Kohlmeyer, A., Moore, S.G., Nguyen, T.D., Shan, R., Stevens, M.J., Tranchida, J., Trott, C., Plimpton, S.J., 2022. LAMMPS - a flexible simulation tool for particle-based materials modeling at the atomic, meso, and continuum scales. Comput. Phys. Commun. 271, 108171. doi:10.1016/j.cpc.2021.108171.

Viesca, J.-L., Anand, M., Blanco, D., Fernández-González, A., García, A., Hadfield, M., 2016. Tribological behaviour of PVD coatings lubricated with a FAP^- anion-based ionic liquid used as an additive. Lubricants 4 (1). doi:10.3390/lubricants4010008.

Voroshylova, I.V., Teixeira, F., Costa, R., Pereira, C.M., Cordeiro, M.N.D., 2016. Interactions in the ionic liquid [EMIM][FAP]: a coupled experimental and computational analysis. Phys. Chem. Chem. Phys. 18 (4), 2617–2628. doi:10.1039/C5CP06027C.

Wang, J., Wolf, R.M., Caldwell, J.W., Kollman, P.A., Case, D.A., 2004. Development and testing of a general amber force field. J. Comput. Chem. 25 (9), 1157–1174. doi:10.1002/jcc.20035.

Wu, H., Shah, J.K., Tenney, C.M., Rosch, T.W., Maginn, E.J., 2011. Structure and dynamics of neat and CO_2 -reacted ionic liquid tetrabutylphosphonium 2-cyanopyrrolide. Ind. Eng. Chem. Res. 50 (15), 8983–8993. doi:10.1021/ie200518f.

Yao, C., Pitner, W.R., Anderson, J.L., 2009. Ionic liquids containing the tris(pentafluoroethyl)trifluorophosphate anion: a new class of highly selective and ultra hydrophobic solvents for the extraction of polycyclic aromatic hydrocarbons using single drop microextraction. Anal. Chem. 81 (12), 5054–5063. doi:10.1021/ac900719m.

Yeh, I.-C., Hummer, G., 2004. System-size dependence of diffusion coefficients and viscosities from molecular dynamics simulations with periodic boundary conditions. J. Phys. Chem. B 108 (40), 15873–15879. doi:10.1021/jp0477147.

Zaitsau, D.H., Verevkin, S.P., 2019. Imidazolium-based ionic liquids containing FAP anion: thermodynamic study. J. Mol. Liq. 287, 110959. doi:10.1016/j.molliq.2019.110959.

Zhang, X., Huo, F., Liu, Z., Wang, W., Shi, W., Maginn, E.J., 2009. Absorption of CO_2 in the ionic liquid 1-n-hexyl-3-methylimidazolium tris(pentafluoroethyl)trifluorophosphate ([hmim][FEP]): a molecular view by computer simulations. J. Phys. Chem. B 113 (21), 7591–7598. doi:10.1021/jp900403q.

Zhang, X., Liu, Z., Wang, W., 2008. Screening of ionic liquids to capture CO_2 by COSMO-RS and experiments. AIChE J. 54 (10), 2717–2728. doi:10.1002/aic.11573.

Zhang, Y., Maginn, E.J., 2012. A simple AIMD approach to derive atomic charges for condensed phase simulation of ionic liquids. J. Phys. Chem. B 116 (33), 10036–10048. doi:10.1021/jp3037999.

Zhang, Y., Otani, A., Maginn, E.J., 2015. Reliable viscosity calculation from equilibrium molecular dynamics simulations: a time decomposition method. J. Chem. Theory Comput. 11 (8), 3537–3546. doi:10.1021/acs.jctc.5b00351.

Zhang, Y., Xue, L., Khabaz, F., Doerfler, R., Quitevis, E.L., Khare, R., Maginn, E.J., 2015. Molecular topology and local dynamics govern the viscosity of imidazolium-based ionic liquids. J. Phys. Chem. B 119 (47), 14934–14944. doi:10.1021/acs.jpcb.5b08245.

Zhang, Y., Zhang, Y., McCready, M.J., Maginn, E.J., 2018. Evaluation and refinement of the general AMBER force field for nineteen pure organic electrolyte solvents. J. Chem. Eng. Data 63, 3488–3502. doi:10.1021/acs.jced.8b00382.